Journal of Alloys and Compounds 935 (2023) 168094

Contents lists available at ScienceDirect

Journal of Alloys and Compounds

journal homepage: www.elsevier.com/locate/jalcom

Investigation of crossed-twin structure formation in magnesium and magnesium alloys

Jiaxiang Wang [a], Mariyappan Arul Kumar [b,*], Irene J. Beyerlein [a,c]

[a] Department of Mechanical Engineering, University of California, Santa Barbara, CA 93106, USA
[b] Materials Science and Technology Division, Los Alamos National Laboratory, Los Alamos, NM 87545, USA
[c] Materials Department, University of California, Santa Barbara, CA 93106, USA

ARTICLE INFO

Article history:
Received 28 August 2022
Received in revised form 1 November 2022
Accepted 14 November 2022
Available online 15 November 2022

Keywords:
Twin-twin interaction
Stress concentration
Crystal plasticity
Dislocations
Pyramidal slip

ABSTRACT

In this work, the effect of alloying addition on the propensity for twin-twin interactions to transform into crossed-twin structures in magnesium alloys is investigated. A full-field elasto-viscoplastic fast Fourier transform (EVP-FFT) framework combined with a discrete twin model and dislocation density-based hardening law for slip strengths is used to calculate the micromechanical fields in the crystalline matrix around the interacting twins. AZ31 and MgLi alloys are selected along with pure Mg to study the influence of plastic anisotropy in connection with alloying elements. These alloys were selected since their plastic anisotropy measure, which is defined as the ratio between the critical resolved shear stress for pyramidal ⟨c +a⟩ and basal ⟨a⟩ slip modes, spanned a wide range. To quantify the role of twin thicknesses, we probe a range of impinging twin thicknesses while fixing the recipient twin thickness. The analysis reveals that: (i) the local driving stress for crossed twin structure formation generated from the interaction of the two twins is lower in a low plastically anisotropic material, like a MgLi alloy, than a high plastically anisotropic material like pure Mg and (ii) the critical impinging twin thickness needed to form the crossed twin structure in pure Mg, AZ31 and MgLi alloys is ~0.5, ~0.75 and ~1.5 times the recipient twin thickness. We propose a relationship between the tendency for crossed twin structure formation and the experimentally observed higher ductility in MgLi alloys compared to pure Mg. One key implication of the findings is that crossed-twin structure formation can be hindered and the ductility of magnesium alloy thereby improved by properly choosing alloying elements that lower the slip strength for pyramidal $\langle c + a \rangle$ slip.

1. Introduction

Magnesium and its alloys are attractive materials for many structural applications where lightweight and high-specific strength engineering components are required [1–3]. The applicability of these alloys is primarily governed by their load carrying capacity and the level of plasticity or ductility. The available slip modes in hexagonal close-packed (HCP) Mg for accommodating plastic deformation are basal $\langle a \rangle$, prismatic $\langle a \rangle$, and pyramidal $\langle c + a \rangle$ [4–6]. The activation stress for the pyramidal slip is so high compared to the other $\langle a \rangle$ slip modes [7]. Thus, the accommodation of straining along the c-axis of the crystal by dislocation slip is limited. In turn, the plasticity is accommodated by a combination of dislocation slip and deformation twinning [8–10]. The wide variation in the activation stress for slip and the activation of directional dependent twinning leads to highly anisotropic and asymmetric deformation responses with limited ductility and formability [9,11–13]. In the last two decades, numerous strategies have been proposed to reduce the plastic anisotropy and to improve the formability. Mainly texture weakening and alloying additions are investigated extensively as plausible strategies. The texture weakening, via prior thermo-mechanical processing, certainly improves the ductility by reducing the activation of deformation twinning [14–16]. However, the texture weakening also reduces the strength of the material, which is not desirable. On the other hand, the alloying addition shows promising benefits on strength, ductility, and anisotropy [17–23]. First, the alloying addition increases the strength of the material via solid solution and precipitate strengthening and controlling the grain/twin boundary sliding and migration [24–28]. Second, the alloying elements lower the c/a ratio of the HCP magnesium lattice and thus increase the activation stress for basal slip, enhancing the activity of non-basal slip [7,29]. Lastly, the addition of alloying elements like Li and rare-earth elements induces significant variation in the stacking fault energy landscapes [30] and facilitates the dissociation and

* Corresponding author.
E-mail addresses: marulkr@lanl.gov, marulkr@gmail.com (M.A. Kumar).

https://doi.org/10.1016/j.jallcom.2022.168094
0925-8388/

formation of $\langle c+a \rangle$ dislocations on the pyramidal plane [7,18,21,31]. However, the formation and interaction of deformation twins in magnesium alloy systems are still significant, which necessitates the understanding of twinning.

Unlike slip, the twins are of volumetric domains within a grain or crystal with significant localized shear and abrupt lattice rotation [5,8,32]. For instance, the most observed $\{10\bar{1}2\}$ tensile twin in magnesium imposes a localized shear strain of ~13% and a lattice rotation of ~86° about the $\langle 1\bar{1}20 \rangle$ direction. Deformation twins in HCP polycrystals most often nucleate at the grain boundaries where the suitable local stress and defects are present [33]. The nucleated twin embryos propagate into the grain and mostly terminate at the opposing grain boundaries or at the precipitates in the precipitate hardened alloys [34–37]. The terminated twins at the grain boundaries can transmit across the boundaries and eventually form a long twin chain [38–41]. Based on the loading direction, in HCP crystals, more than one crystallographically equivalent twin variant can be activated [42,43]. For example, a tensile loading along the c-axis of the crystal can equally activate all six twin variants. Thus, the formation of deformation twins can introduce the following interactions: twin-slip, twin-precipitates, twin-grain boundaries, and twin-twin. All these interactions affect the strength and ductility of the material systems and also the microstructural evolution [22,44–50]. In this work, we focus on twin-twin interactions (TTI) in Mg alloys.

The activation of non-parallel twin variants leads to the formation of twin-twin junctions (TTJ) and a complex 3D network structure [42–44]. Based on the zone axes of the constituting twins, $\{10\bar{1}2\}$ twin-twin junctions are classified as co-zone (twin variants sharing the same zone axis) or non-co-zone (two twin variants with different zone axes). The formation of TTJs is commonly observed in magnesium and its alloys. In the 1960′s Roberts and Partridge experimentally characterized the accommodation that occurs around interacting tensile twins in magnesium [10]. The TTI is known to affect the strain hardening response and failure of the material [43,44,47,49–51]. Specifically, the twin-twin interactions can play a distinctive role compared to isolated twins in their interactions with glide dislocations, twin propagation, and local strain hardening. For example, Yu et al. showed that the increase in yield strength and strain hardening under cyclic loading is primarily due to the increases in the number of TTJs [43]. El Kadiri et al. compared the twin nucleation and growth behavior in grains with single and two non-parallel variants [52]. They found that the grain with the two non-parallel twin variants, that are formed by prismatic plane normal direction compression, had a higher twin nucleation rate and lower twin thickening rate than the grain that formed only one twin variant by $\langle a \rangle$-axis compression loading. Chen et al. observed abnormal twin boundary migration on both sides of the TTJ using in-situ electron backscattered diffraction [53]. Morrow et al. found that the presence of TTJs retards the detwinning process under cyclic loading [54,55]. Furthermore, the TTI sites are known to nucleate cracks in many material systems, including cubic and hexagonal structure materials. In the 1960 s, Reid showed that the microcracks nucleate at the TTI site in body-centered cubic (BCC) iron and iron-silicon alloys [56,57]. Recently, via in-situ characterization of microstructures, Russell et al. showed that the twin-grain boundary and twin-twin interactions develop large cracks in HCP magnesium alloy [58]. With that being said, the twin-twin interactions do improve the material's performance. For example, the presence of twin-twin junctions weakens the crystallographic texture during recrystallization [59]. Also, it has been shown that the formation of several twin crossings increases the strength of the material by reducing the mean free path for dislocation motion while maintaining the ductility [60–63]. Thus, understanding the formation of TTJs is paramount to assess and improve the performance of Mg alloys.

The experimental literature often reports observations of crossed twin structures in Mg or Mg alloys [37,43,52,64,65]. In this configuration, the two twins appear to interpenetrate, wherein the same twin variant of one twin lies on both sides of another twin. Crossed twins have two twin-twin junctions (TTJs) and hence increased chances of nucleating cracks. Existing numerical studies of TTIs mainly focus on one twin interacting with another [66–70], but less so on the formation of crossed twin structures. Using the crystal plasticity model, Kumar et al. recently proposed a mechanism for the formation of a crossed twin structure from a TTJ [68]. They showed that the local stress field created by the impinging twin may help to create a new twin on the opposite side of the junction. Upon further loading, these two now crossed twins grow by the thickening. Thus, a cross-twinned structure forms by the impinging twin "hopping" over the recipient twin, rather than transmitting into and out of the recipient twin. With the general process recently understood, the factors that can influence the formation of crossed-twin structures have not been explored, such as the effect of alloying additions or relative thicknesses of the two participating twins.

In this work, using the crystal plasticity modeling approach, we investigate the effect of the thickness of the interacting twins and the plastic properties of the Mg alloy induced local stresses. The stress fields around two interacting co-zone twins are calculated using a computational model that is built on the elasto-viscoplastic fast Fourier transformation (EVP-FFT) framework and incorporates a model for discrete twin domains and for dislocation density-based hardening model for the critical resolved shear stress (CRSS) values for slip systems [27,71–74]. To elucidate the effect of alloying additions, we consider pure Mg and two Mg alloys, Mg-4Li and AZ31. To investigate the role of twin thicknesses on crossed twin, the calculations are repeated for a range of twin thicknesses. Analysis of the local stress fields and dislocation densities finds that the local stress that encourages crossed twin structure formation increases with the thickness of the impinging twin and is highly sensitive to the alloying addition. The critical impinging twin thickness needed for crossing structure formation is lower in the more plastically anisotropic pure Mg compared to the plastically less anisotropic MgLi alloy.

2. Numerical method

2.1. The crystal plasticity model

In this work, the EVP-FFT model with dislocation density-based constitutive law is used. The original FFT-based method was developed to study the local and effective mechanical response of nonlinear composite materials [75]. Later, it was adapted by Lebensohn to study polycrystalline materials [76]. Over the years, the FFT approach has been extended to apply to many distinct deformation regimes for such materials, such as elasticity [77], incompressible visco-plasticity [78], and infinitesimal elasto-visco-plasticity [79]. Here, we use the infinitesimal elasto-viscoplasticity model along with the following additions: 1) module for explicit twinning shear transformation simulation [73,74] and 2) dislocation density-based hardening law [80]. The EVPFFT framework, constitutive model, and hardening laws are briefly revisited here.

Under an infinite strain approximation, the elasto-viscoplastic constitutive behavior of the materials is written as,

$$\sigma(x) = \boldsymbol{C}(x): \quad \varepsilon^{el}(x) = \boldsymbol{C}(x): \left(\left(\varepsilon(x) - \varepsilon^{pl}(x) - \varepsilon^{tr}(x)\right)\right) \tag{1}$$

where $\sigma(x)$, $\boldsymbol{C}(x)$, $\varepsilon^{el}(x)$ are the Cauchy stress tensor, elastic stiffness tensor, and elastic strain at a material point x, respectively. In this expression, the elastic strain is the difference between total strain $\varepsilon(x)$ and the sum of the plastic strain $\varepsilon^{pl}(x)$ and transformation strain $\varepsilon^{tr}(x)$. Using an implicit time discretization scheme, the stress tensor at time $t + \Delta t$ is given by,

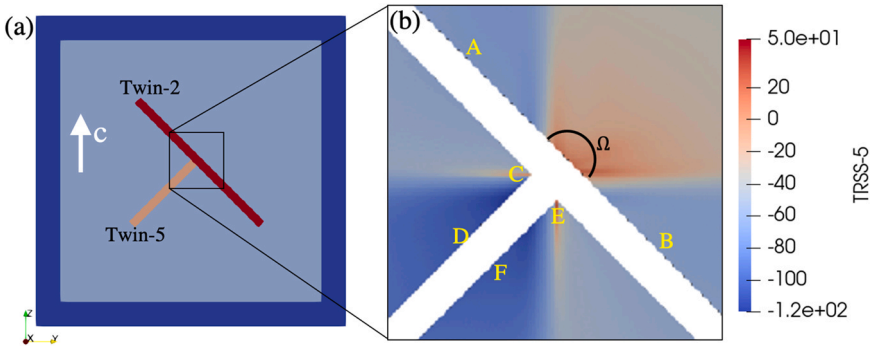

Fig. 1. (a) Schematic of the EVPFFT unit cell for TTI simulations. The central parent grain contains the recipient twin (T2) and the impinging twin (T5). (b) Model calculated twin plane resolved shear stress (TRSS) distribution in pure Mg with TR=IT_t/RT_t = 1 after forming the twin-twin junction.

$$\sigma^{t+\Delta t}(x) = \quad \boldsymbol{C}(x)\colon(\varepsilon^{t+\Delta t}(x) - \varepsilon^{pl,t}(x) - \dot{\varepsilon}^{pl,t+\Delta t} \quad (x, \sigma^{t+\Delta t})\Delta t - \varepsilon^{tr,t}(x) - \Delta\varepsilon^{tr,t+\Delta t}(x)) \tag{2}$$

where $\dot{\varepsilon}^{pl}$ is the viscoplastic strain rate, and it is assumed to be accommodated by dislocation glide. In turn, the $\dot{\varepsilon}^{pl}$ is constitutively related with the stress at material point x through the summation over N active slip systems, of the form:

$$\dot{\varepsilon}^{pl}(x) = \dot{\gamma}_0 \sum_{s=1}^{N} \mathbf{m}^s(x) \left| \frac{\mathbf{m}^s\colon \sigma}{\tau_c^s(\dot{\varepsilon}, T)} \right|^n \mathrm{sign}(\mathbf{m}^s\colon \sigma) \tag{3}$$

where τ_c^s is the critical resolved shear stress. A dislocation density-based hardening scheme is used to evolve τ_c^s with strain as a function of the imposed strain rate $\dot{\varepsilon}$ and temperature T. The term $\mathbf{m^s}(\mathbf{m^s} = 0.5(\ \ (\mathbf{b^s} \otimes \mathbf{n^s} + \mathbf{n^s}\mathbf{b^s})))$ is the symmetric part of the Schmid tensor, where $\boldsymbol{b^s}$ and $\boldsymbol{n^s}$are two orthonormal unit vectors representing the slip direction and slip plane normal, respectively. The shear rate $\dot{\gamma}_0$ is a normalization factor, and n is the rate-sensitivity exponent.

The twin transformation strain within the explicit twin domain is imposed via successive increments using:

$$\Delta\varepsilon^{tr}(x) = \boldsymbol{m}^{tw}\Delta\gamma^{tw}(x) \quad = \mathbf{m}^{tw}\frac{s^{tw}}{N^{twincr}} \tag{4}$$

where $\boldsymbol{m}^{tw}$ is the Schmid tensor associated with the explicitly simulated twin system, s^{tw} and N^{twincr} are the characteristic twin shear and number of increments, respectively.

Following the work of [80], the critical resolved shear stress (CRSS) is expressed in terms of dislocation density as:

$$\tau_c^s = \tau_0 + b^s\chi\mu\sqrt{\rho_{for}^s} + k_{deb}\mu b^s\sqrt{\rho_{deb}}\log\left(\frac{1}{b\sqrt{\rho_{deb}}}\right) \tag{5}$$

Here, τ_0 is the initial slip resistance that depends on slip mode, solute density, temperature, and strain rate. The second and third terms represent work hardening due to dislocation interactions. In the above equation the terms χ, μ, k_{deb}, ρ_{for}, ρ_{deb} are, respectively, the interaction coefficient, shear modulus, material-independent constant, forest dislocation density and debris dislocation density. The following equation governs the evolution of dislocation density:

$$\frac{\partial\rho}{\partial\gamma} = \frac{\partial\rho_{gen}}{\partial\gamma} - \frac{\partial\rho_{deb}}{\partial\gamma} - \frac{\partial\rho_{ann}}{\partial\gamma} \tag{6}$$

which states that the rate of accumulated dislocation equals the difference between the rate of generation and the rate of removal, which includes the dislocation density that converts to sessile debris, ρ_{deb}, and that is annihilated, ρ_{ann}. We refer the reader to [80] for more details of the constitutive law and dislocation density evolution.

2.2. Model setup and numerical simulations of TTI

The EVP-FFT model setup for the TTI simulations is shown in Fig. 1(a). The unit cell is periodic in all three directions and consists of a parent matrix grain (light blue) containing the TTJ and the surrounding buffer layer (dark blue). The unit cell is discretized into 3 × 500×500 voxels with 40 voxels thick buffer layer. The crystal orientation of each voxel in the buffer layer is randomly assigned. The crystallographic orientation of matrix grain is taken as (0°,0°,0°) in the Bunge convention, which aligns the Y and Z axes with the [01$\bar{1}$0] and [0001] directions of the matrix grain. The voxels with red and orange colors designate explicit twin domains of variant T2-(01$\bar{1}$2)[0$\bar{1}$11] and T5-(01$\bar{1}$2)[0$\bar{1}$11], respectively. We will refer to them as the recipient twin (RT) and impinging twin (IT). The twinning plane normal and shear direction of both twins are in the YZ plane. There is no out-of-plane twin shear in XY and XZ planes. Because of this, considered 2D columnar microstructure is sufficient.

The unit cell is subjected to a compression strain of 0.5% along the Y direction while applying stress-free boundary conditions in the Z and X faces. This imposed stress state corresponds to a Schmid factor of nearly 0.5 for both the twin variants. Though the chosen initial strain value is arbitrary, but it is sufficient to activate twins in all three material systems. Further, the effect of this initial strain value on the derived qualitative concussions reported in the following sections is minimal. It is confirmed by repeating a few calculations at 1% initial strain level. For the sake of compactness, those calculation results are not shown. After the initial pre-straining, the RT is introduced first in the preselected domain by reorienting the crystal following the twinning relationship and imposing the characteristic twinning shear of 12.9% over 1000 numerical steps at a fixed macroscopic boundary condition. Then, the IT is formed at the same macroscopic loading. Though the twin formation is a sequential stochastic process, for the sake of simplicity, the static twins are introduced in the pre-selected regions. Following our recent work, the considered rectangular twin shape is expected to have less effect on the calculated micromechanical fields [81]. In all simulation stages, the deformation is accommodated by a combination of anisotropic elasticity and slip-dislocation mediated plasticity. The details of elasticity, plastic deformation modes, and the associated parameters are given in the next section.

The EVP-FFT simulations with different twin thicknesses are performed to understand the effect of relative twin sizes on TTI induced local stresses. Accordingly, for a fixed recipient twin thickness (RT_t = 12 voxels), the impinging twin thickness (IT_t) is varied. The considered impinging twin thicknesses are 3, 6, 9, 12, 15, and 18 voxels, which corresponds to the thickness ratios (TR) of $TR = IT_t/RT_t$= 0.25, 0.5, 0.75, 1.0, 1.25 and 1.5. These thickness ratios cover different stages of TTI, starting with the thin impinging twin ($TR < 1$) to the expanded one ($TR > 1$).

Table 1
Chemical composition of studied Mg alloys and the corresponding CRSS values along with PA ratio.

Mg alloys	Composition (wt%)			CRSS at 0.5% strain before twinning [MPa]				PA	Ref.
	Al	Zn	Li	Basal	Prismatic	Pyramidal	T. Twin		
Pure Mg	–	–	–	3.85	36.2	87.2	11	22.7	[87]
AZ31	3.0	1.0	–	12.1	47.3	158.0	13	13.1	[88]
MgLi	–	–	4.0	5.5	17.1	53.0	25	9.6	[64]

2.3. Materials selection and the associated parameters

The most common wrought AZ31 and magnesium-lithium (MgLi) alloys are selected to study the effect of alloying additions on the TTI. Pure Mg is also considered as a reference case. These Mg alloys are potential alternatives to aluminum alloys, and readily available in different forms, such as plate, sheet, and bar [82–84]. The chemical compositions of these alloys are given in Table 1. Since the effect of alloying elements on the lattice parameters and elastic constants is commonly considered minimal [85,86], we can reasonably use the lattice parameter, c/a ratio, and anisotropic elastic constants for Mg for all alloys. Accordingly, c/a= 1.624, and the anisotropic elastic constants in GPa are: $C_{11} = 59.5$; $C_{12} = 26.1$; $C_{13} = 21.8$; $C_{33} = 65.6$ and $C_{44} = 16.3$ [86]. For plastic deformation, three slip modes, basal ⟨a⟩, prismatic ⟨a⟩ and pyramidal ⟨c+a⟩ are made available. The initial CRSS and the associated hardening parameters for these slip modes for Mg and two alloys are taken from [64,87,88]. The values from these works are directly taken because they have used the same (i) deformation framework (infinitesimal strain formulation), (ii) set of plastic dissipative slip modes (basal < a >, prismatic < a > and pyramidal < c+a >), (iii) constitutive law for slip activity (power law equation with strain rate sensitivity, n), and (iv) strain hardening model (DD-based hardening law) as in the present work. Thus, there is no need to re-characterize them here. Furthermore, note that these values in [64,87,88] are obtained by fitting the experimental stress-strain responses and texture evolution for several macroscopic loading conditions like tension and/or compression along different directions.

A plastic anisotropy (PA) measure is proposed to quantify the effect of alloying on plasticity. It is well documented that the plastic anisotropy in the HCP materials is primarily governed by the differences in the CRSS values between basal and non-basal slip modes. Both the prismatic < a > and pyramidal ⟨c+a⟩ slip modes are non-basal. However, between these two slip modes, only the pyramidal ⟨c+a⟩ slip can accommodate the c-axis deformation and hence for the PA calculation, pyramidal ⟨c+a⟩ slip considered the key non-basal slip mode. Based on this, we define the PA measure as the ratio between the CRSS values of pyramidal ⟨c+a⟩ and basal ⟨a⟩ slip modes. Similar or slightly modified measures have been proposed in the literature to study the effect of anisotropy in slip plasticity on tension-compression asymmetry and the twinning process [89–92]. Using the initial CRSS values, the PA measure for pure Mg is 25.9 ($\tau_0^{\text{Basal}} = 3.33$MPa and $\tau_0^{\text{Pyramidal}} = 86.2$MPa [87]); for AZ31 is 13.5 ($\tau_0^{\text{Basal}} = 11.6$MPa and $\tau_0^{\text{Pyramidal}} = 157.0$MPa [88]), and for MgLi is 10.4 ($\tau_0^{\text{Basal}} = 5.0$MPa and $\tau_0^{\text{Pyramidal}} = 52.0$MPa [64]). According to the PA, the AZ31 and MgLi alloys are plastically less anisotropic than pure Mg and MgLi is less anisotropic than AZ31. Since the CRSS values will evolve with deformation, the PA measure will change accordingly. Table 1 shows the PA measure calculated using the instantaneous CRSS values after pre-straining, or just before the TTI calculations. Apart from the slight changes in the PA measure values, the order of plastic anisotropy among these three material systems remains the same.

3. Results

3.1. Twin-twin interaction induced local stresses

The EVP-FFT model calculates the full stress and strain tensor at every material point and at every strain step in the simulation. For our analysis, we analyze the full stress and strain field at three key steps: after pre-straining, after recipient twin formation, and finally after TTJ formation (which means forming the impinging twin with the recipient twin present). The latter case is the most pertinent for understanding the TTI-induced local stresses for crossed twin structure formation. From the stress tensor, the twin plane resolved shear stress (TRSS) for a given twin variant is calculated since it drives the activation for twin embryo formation, twin tip propagation, and twin boundary migration. The TRSS values are calculated for all six variants. The recipient twin variant is variant-2 (V2) and the impinging twin variant is variant-5 (V5), which share the same shear zone. Fig. 1(b) shows TRSS distribution for V5 (TRSS-5) surrounding the co-zone TTJ in pure Mg. The thicknesses of the intersecting twins are equal, with a thickness ratio (TR) = $IT_t/RT_t = 1$. The twin domains are removed from the visualization, and the TRSS distribution shown only focuses on where the two twins meet. Although not shown, at the pre-strain level and before forming the twins, the TRSS fields for both V2 and V5 are homogeneous, and the values are positive and higher than the CRSS. As shown in Fig. 1(b), after forming the TTJ, the TRSS-5 field becomes highly heterogeneous. This TRSS distribution shown in Fig. 1(b) is consistent with the previous studies on co-zone TTJs, which only considered $IT_t/RT_t = 1$ [66,68,93]. On the impingement side and along the impinging twin boundaries, the TRSS-5 value is negative. The growth of the impinging twin is thus unlikely without any further macroscopic loading. The TRSS-5 in a localized region on the opposite side of the TTJ is, however, higher than the CRSS value (=11 MPa). The nucleation of an IT variant twin here would be favored, and should it occur, it would lead to a crossed twin structure.

To check the possibility of forming other twin variants, Fig. 2 shows the TRSS profile along the recipient twin boundary from point A to B, as marked in Fig. 1(b). The position along the RT boundary is normalized with the RT thickness and the TRSS values are normalized with respect to the twin CRSS value given in Table 1. The two vertical dashed lines in Fig. 2 correspond to the points in the RT top boundary where the IT boundaries intersect the RT. The profiles indicate that the twin-twin interaction locally increases the TRSS values for all the variants compared to those without the twins. The TRSS for the RT and IT variants, however, are higher compared to those of the other variants. Thus, either the RT can grow locally, or a new twin of the IT variant can form on the top boundary of the RT. This observation agrees with the experimental observations in single crystal pure Mg, AM30, and AZ91 alloy [37,43,52,65]. These experimental studies found that the variant of the twin formed on the opposite side of the $\{10\bar{1}2\}$ tensile twin co-zone junction is the same as of the impinging twin. Hereinafter, only the TRSS field for the IT variant is studied in detail.

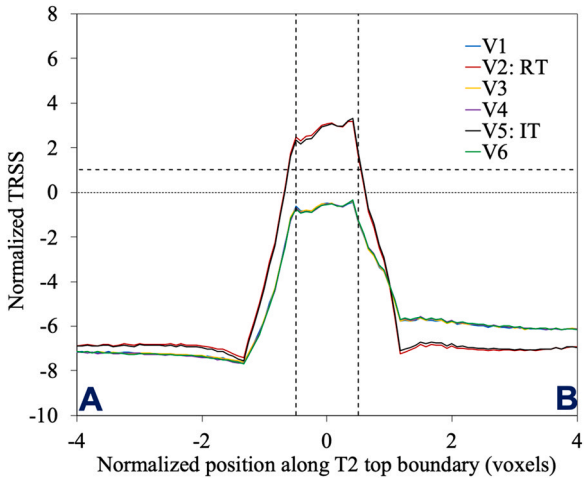

Fig. 2. The model calculated TRSS profile (normalized with twin CRSS value) in pure Mg with TR = lT_t/RT_t = 1 along the RT boundary for all six twin variants. The position is normalized with the RT thickness. Variants 2 and 5 correspond to the RT and IT, respectively. The vertical dashed lines correspond to the points where IT would impinge on RT top boundary. See Fig. 1(b) for positions A and B.

3.2. Crossed twin structure: effect of twin thicknesses

In this section, we study the effect of TTJ twin thicknesses on the TRSS boundary stresses that would drive IT (V5) expansion. Fig. 3 shows the change in the TRSS-5 profile along the RT top boundary with varying IT thicknesses for pure Mg. As before, the TRSS-5 is normalized with respect to the twin CRSS. To help visualization, only the TRSS profiles for IT thickness ratios of 0.25, 0.5, 1.0, and 1.5 are shown. The vertical dashed lines correspond to the points in the RT top boundary where IT would impinge on RT. For reference, the TRSS-5 profile is also shown for the case with TR= 0.0, corresponding to a crystal with only the RT and not the IT. In the TR= 0.0 case, the TRSS values are negative, in the anti-twin shear sense. Thus, a new IT twin is unlikely to form at the RT top boundary of the RT. From the TRSS-5 profile in Fig. 3 with the interacting the IT and RT twins, a high TRSS concentration develops within a narrow region in the RT top boundary. The degree of localization intensified with increasing IT thickness. For *TR* of 0.5 and greater this value exceeds the CRSS. The apparent crossed twin structure formation is, therefore, possible for IT thicknesses slightly higher than half of the RT thickness.

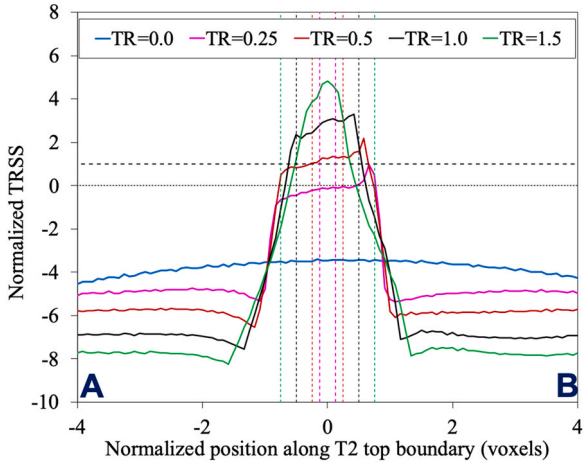

Fig. 3. Effect of constituting twins' thicknesses on stress localization for crossing structure formation. TR= 0 corresponds to the case where there is no impinging twin. IT thickness is varied in terms of RT thickness from 0.25 to 1.5. The vertical dashed lines represent the points in which IT would impinge on RT top boundary and are colored following the IT thickness cases.

3.3. Crossed twinned structure: effect of alloying additions

The effects of alloying on the TTI-induced local stresses and the minimum thickness ratio needed for creating the crossed twin structure is studied here. Fig. 4(a) compares the TRSS-5 profiles along the top boundary of the RT for all three material systems for a twin thickness ratio of 1.0. The TRSS-5 values are normalized with the corresponding twin system CRSS values from Table 1. Fig. 4(a) reveals that, for a similar TTI configuration, the stress localization that may drive the formation of a new twin on the RT top boundary is highest in pure Mg. For MgLi, this stress concentration is lower than 1.0 implying that crossed twin structure formation is not favored compared to the AZ31 alloy. The possibility of crossed twin structure formation is directly correlated with the material PA (see Table 1). The more plastically anisotropic the material the more likely cross-twinning is.

To identify the minimum twin thickness ratio needed for crossed twin structure formation, we have calculated the average TRSS-5 in a small region of radius 3 voxels, Ω, shown in Fig. 1(b), in the vicinity of the IT tip at the RT top boundary. The average TRSS-5 values normalized with the corresponding CRSS values for all three materials systems are plotted in Fig. 4(b) as a function of thickness ratio. The value at which the normalized TRSS reaches the value of one in pure Mg, AZ31, and MgLi alloy is 0.5, ~0.75, and ~1.5, respectively. It suggests that to nucleate a new twin at the RT top boundary, the IT needs to be thicker in plastically less anisotropic materials, like MgLi, than that in more anisotropic materials, like pure Mg.

3.4. Possibility of impinging twin growth

Twin-twin junction formation usually involves an IT that newly propagates into the grain and impinges on the RT. As such the IT is most often thinner than the RT, except for a few favorable loading conditions when the thicknesses of the IT and RT are comparable [94]. Thus, the IT/RT twin thickness ratio most likely be less than one. As mentioned in the previous section, the critical thickness ratio needed for twin crossing to occur in MgLi alloy is higher than one, whereas in pure Mg and AZ31 twin can cross for thickness ratios less than one. Thus, the subsequent growth of the crossed twin structure formation in MgLi alloys is possible only if the IT grows. To check whether the IT can grow in MgLi alloy, Fig. 5 studies the TRSS-5 profiles along the left and right boundaries of IT (as marked in Fig. 1(b)) for the MgLi alloy. The TRSS-5 in the reference, isolated RT case is negative. For all non-zero IT thicknesses, the twin-twin junction lowers the TRSS-5. This suggests that IT thickening is unlikely without increasing the macroscopic loading. However, increases in the macroscopic loading could also help grow the RT. As a result, the twin thickness ratio could remain low and in turn, the formation of a crossed twin structure in MgLi alloy is unlikely.

4. Discussion

In this study, the effect of alloying additions on the possibility and minimum twin thickness ratio needed for crossed-twin structure formation is numerically studied. In a plastically less anisotropic material like MgLi alloy, the driving force for forming a crossed-twin structure associated with the stress concentrations developed from the intersections of the IT and RT is less, and the minimum IT thickness needed is high. The situation is reversed for a plastically high anisotropic material like pure Mg, and so in such materials, crossed twins can be achieved even for relatively thin ITs. The dependence on plastic anisotropy is directly correlated with the availability of pyramidal ⟨c+a⟩ slip. For example, in MgLi alloy, the difference in the CRSS values of basal ⟨a⟩ and pyramidal ⟨c+a⟩ slip is low compared to pure Mg, and so the twin-induced stresses are more easily relaxed by pyramidal slip and the stress concentration

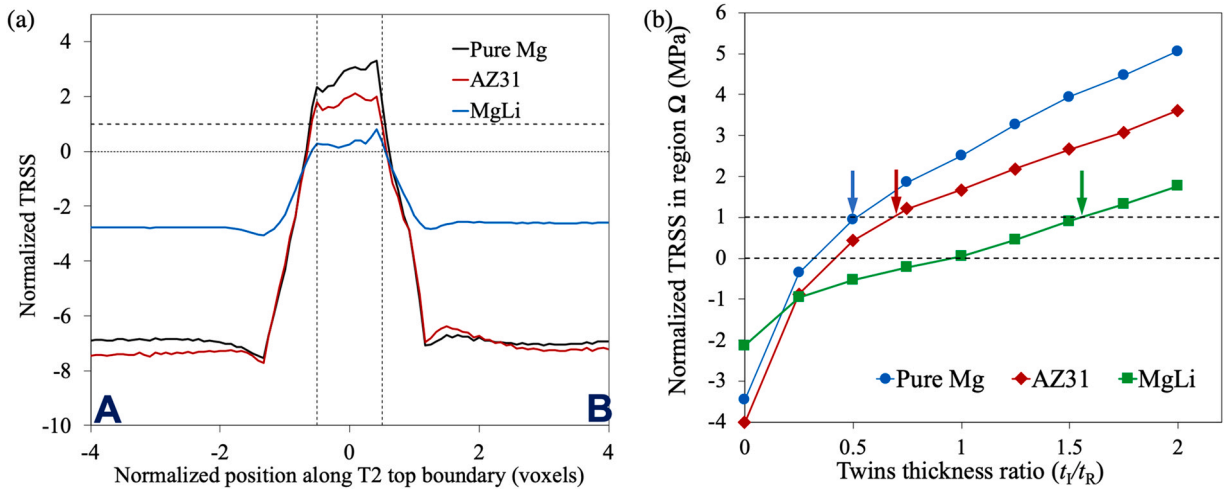

Fig. 4. (a) Effect of alloying addition on the TTI-induced driving stress for crossing structure formation. The TRSS profiles correspond to the case of TR= 1.0. (b) The variation in the localized TRSS in region Ω as a function of twin thickness ratios. Here the TRSS values for each material system are normalized with its corresponding twin CRSS values.

for crossed twinning reduced. In pure Mg, the activation of pyramidal ⟨c+a⟩ slip is limited, and so the twin-twin interaction develops large stress concentrations, favoring crossed-twin structure formation.

Next, we analyze the dislocation densities associated with the stress-fields around the TTJ. Fig. 6(a) shows the dislocation densities for the prismatic, basal, and pyramidal slip modes as a function of twin thickness ratios in MgLi alloy. Here the slip-mode dislocation densities are calculated by adding the dislocation densities of individual slip systems belonging to the same mode, e.g., the basal mode dislocation density is the sum of the densities developed in all three basal slip systems. In Fig. 6(a), the dashed, dotted, and dashed-and-dotted lines correspond to the matrix domain, RT, and IT, respectively, whereas the solid lines show the total dislocation density in the entire unit cell. For all slip modes and for all domains of interest, such as matrix, RT, and IT, the dislocation density significantly increases upon TTJ compared to the case of an isolated RT, i.e., twin thickness ratio of zero. This is consistent with the concept of TTJ-induced formation of defects and strain hardening, reported in [42,43,52,54,59,65,67,69,93,95]. Further, the dislocation density slightly increases with the twin thickness ratio. To understand the effect of alloying additions, the change in the total dislocation density (combining all three modes) for all three material systems with twin thickness ratios is plotted in Fig. 6(b). The total dislocation densities are normalized with respect to that for the isolated RT twin case. Fig. 6(b) clearly reveals that the increase in dislocation density due to TTJ is significantly higher in the MgLi alloy compared to pure Mg and the AZ31 alloy. Evidently, accommodation of TTJ-induced local stresses by slip dislocations dominates in MgLi. To correlate dislocation activity with twin-crossed structure formation, the dislocation densities are calculated in a small region at the tip of the IT on the RT boundary, i.e., in the Ω region marked in Fig. 1(b), where a new twin could form and lead to a crossed-twin structure. Fig. 6(c) shows the basal, prismatic, and pyramidal dislocation densities in the MgLi alloy. The results suggest that pyramidal ⟨c+a⟩ dislocations mainly accommodate the TTJ-induced stresses. Like Fig. 6(b), the total dislocation density ratio in region Ω is plotted for all three material systems in Fig. 6(d). The activation of dislocations in region Ω is significantly higher in the MgLi compared to other material systems, suggesting a reduced propensity of crossed-twin structure formation. The primary difference among these three material systems is only on the difference between the CRSS of the ⟨a⟩ and ⟨c+a⟩ slip modes. Thus, this indicates that crossed-twin structure

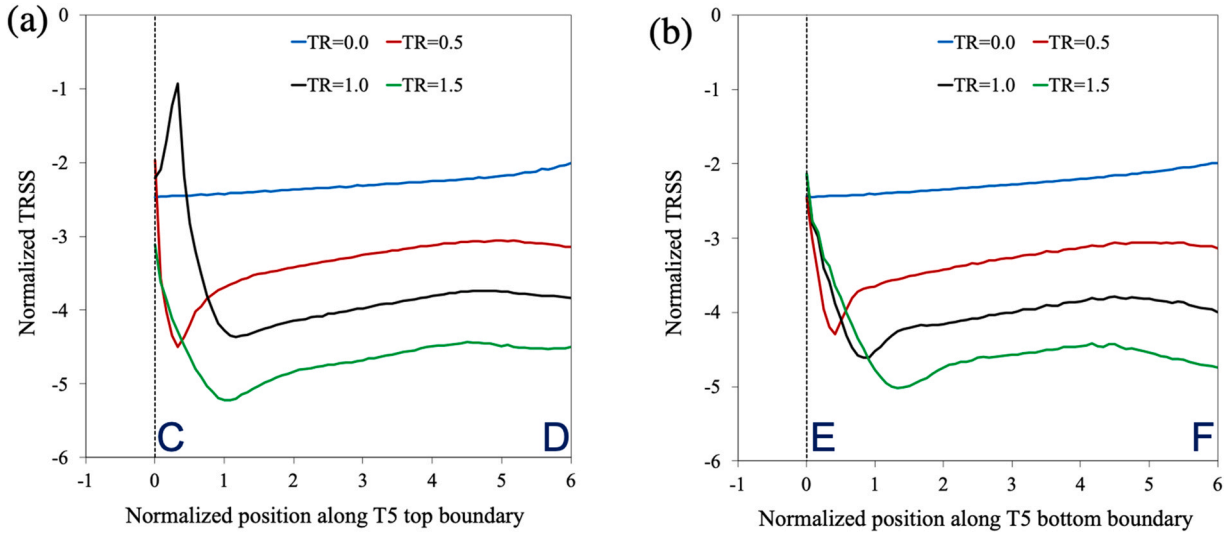

Fig. 5. The model calculated normalized TRSS profiles along the (a) left and (b) right boundary of IT in MgLi alloy for various twin thickness ratio cases. The position along the IT boundary is normalized with RT thickness.

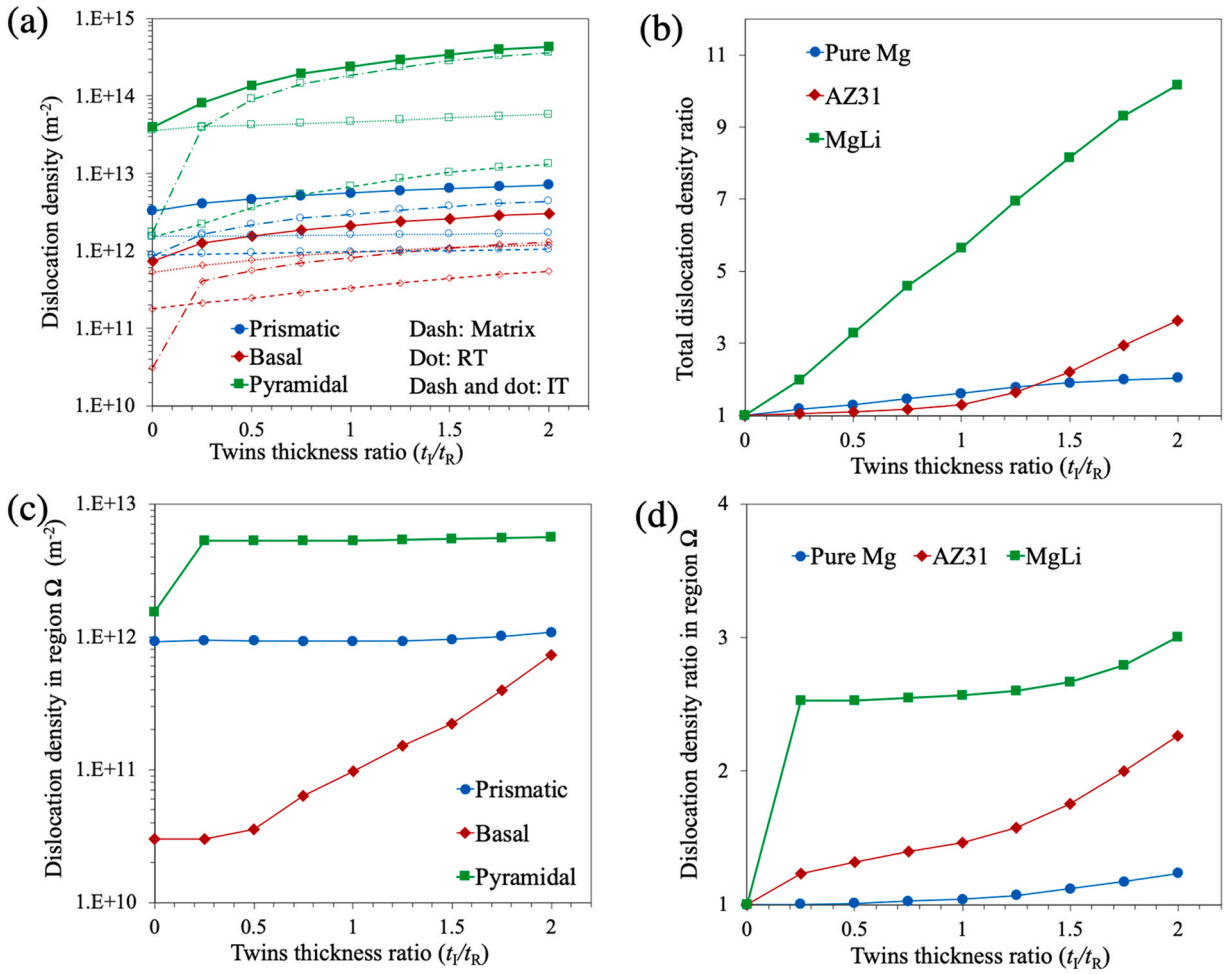

Fig. 6. The effect of twin-twin interaction and alloying addition on dislocation densities. (a) Variation in the model calculated prismatic (blue), basal (red) and pyramidal (green) slip dislocations density in MgLi alloy. The dislocation density in the matrix domain (dashed lines), RT (dotted lines), and IT (dash and dotted lines) are also shown. (b) Variation in the normalized total dislocation density (sum of prismatic, basal, and pyramidal modes) for all three material systems. (c) Changes in the prismatic, basal, and pyramidal dislocation density in the region Ω, marked in Fig. 1(b), for MgLi alloy. (d) Effect of impinging twin thickness on the normalized total dislocation density in the region Ω for all three materials.

formation can be controlled by tailoring the CRSS difference between the basal and pyramidal ⟨c+a⟩ slip modes.

The reported findings can rationalize the experimentally reported ductility in pure Mg, AZ31, and MgLi alloys. The ductility, i.e., the tensile strain to failure, for pure Mg varying between ~10% and ~20% [7,17,96], for AZ31 ranges from ~25–30% [17,44,97], and for MgLi alloy is higher than 35% [7,17,64,98]. It is well documented in the literature that the crack will most likely nucleate at the twin-twin interaction sites [47,49,50,58]. Accordingly, the failure of the component can be directly correlated with the number of twin-twin interaction sites in the material. When a twin-twin junction changes to a crossed-twin structure with strain, the number of sites changes from two to four. The EVP-FFT model calculations suggest that this is more likely in pure Mg than in MgLi and AZ31 alloys, leading to more twin-twin interaction sites in pure Mg than in AZ31 and MgLi alloys. The implication is that the ductility of magnesium alloy can be improved by properly choosing an alloying element that lowers the activation stress required for pyramidal ⟨$c + a$⟩ slip via preventing the crossed twin structure formation.

5. Conclusions

The effect of alloying addition and the constituting twin thicknesses on the development of twin crossed structure formation in magnesium is studied. A full-field elasto-viscoplastic fast Fourier transform (EVP-FFT) framework combined with a discrete twin model and dislocation density-based hardening law for slip strengths is employed to simulate the twin-twin interactions. AZ31 and MgLi alloys are selected along with pure Mg to study the influence of plastic anisotropy in connection with alloying elements. Twin-twin interaction simulations are performed for a range of impinging twin thicknesses while fixing the recipient twin thickness to study the influence of twin thicknesses on crossed structure formation. This detailed study provides the following key findings.

- In a plastically less anisotropic material like MgLi alloy, the driving force for forming a crossed-twin structure associated with the stress concentrations developed from the intersections of the IT and RT is less compared to plastically more anisotropic pure Mg and AZ31 alloy.
- The minimum IT thickness needed to form the crossed twin structure in pure Mg, AZ31, and MgLi alloys is ~0.5, ~0.75, and ~1.5 times the recipient twin thickness. These minimum IT thickness ratios are scaling with the plastic anisotropy.
- Since the dependence on plastic anisotropy is directly correlated with the availability of pyramidal ⟨c+a⟩ slip in comparison with ⟨a⟩ slip, the crossed twin structure formation can be controlled by tailoring the CRSS difference between the basal and pyramidal ⟨c +a⟩ slip modes.

- The model predictions help to rationalize the experimentally reported ductility in pure Mg, AZ31, and MgLi alloys. Specifically, the TTI simulations find that ductility of the material system can be directly correlated with the plastic anisotropy via the propensity for the formation of crossed twin structures. Finally, this work suggests that the ductility of magnesium alloy can be improved by properly choosing an alloying element that lowers the activation stress required for pyramidal $\langle c+a \rangle$ slip via preventing the crossed twin structure formation.

CRediT authorship contribution statement

Jiaxiang Wang: Formal analysis, Investigation, Writing – review & editing, Visualization. **Mariyappan Arul Kumar:** Conceptualization, Methodology, Formal analysis, Writing – original draft, Visualization, Supervision, Funding acquisition. **Irene J. Beyerlein:** Conceptualization, Writing – review & editing, Supervision, Funding acquisition, Project administration.

Appendix A1

See Table A1.

Data availability

Data will be made available on request.

Declaration of Competing Interest

The authors declare that they have no known competing financial interests or personal relationships that could have appeared to influence the work reported in this paper.

Acknowledgments

M.A.K. acknowledges financial support from the U.S. Dept. of Energy, Office of Basic Energy Sciences Project FWP 06SCPE401. J. X. W. and I.J.B. acknowledge financial support from the National Science Foundation under Grant Number 2051390.

Table A1
The DD-based strain hardening model parameters taken from [64,87,88] for pure Mg, AZ31, and MgLi alloys. Here B, Pr and Py refer to basal $\langle a \rangle$, prismatic $\langle a \rangle$ and pyramidal $\langle c+a \rangle$, respectively.

	Pure Mg			AZ31 alloy			MgLi alloy		
	B	Pr	Py	B	Pr	Py	B	Pr	Py
Burgers vector value, b_s (Å)	3.21	3.21	6.12	3.21	3.21	6.12	3.21	3.21	6.12
Initial slip resistance, τ_0 (MPa)	3.33	35.7	86.2	11.6	47.1	157.7	5	14	52
Drag stress, D (MPa)	600.0	7980.0	24,330.0	100.0	150.0	225.0	3500.0	2500.0	3300.0
Normalized activation enthalpy, g	3.36e-3	3.36e-3	3.36e-3	6.4e-4	1.2e-4	6.2e-4	3.3e-3	3.3e-3	9.0e-3
Creation rate, K_1 (1/m)	6.7e9	8.0e9	7.2e9	6.0e6	9.8e7	1.5e8	1.5e8	2.5e8	5.5e9
Reference strain rate, $\dot{\epsilon}_0$ (1/s)	1.0e7	1.0e7	1.0e7	1.0e7	1.0e7	1.0e7	1.0e7	1.0e7	1.0e7

References

[1] N.J. Kim, Critical Assessment 6: Magnesium sheet alloys: viable alternatives to steels? Mater. Sci. Technol. 30 (2014) 1925–1928.
[2] M.K. Kulekci, Magnesium and its alloys applications in automotive industry, Int. J. Adv. Manuf. Technol. 39 (2008) 851–865.
[3] T.M. Pollock, Weight loss with magnesium alloys, Science 328 (2010) 986–987.
[4] B.-Y. Liu, F. Liu, N. Yang, X.-B. Zhai, L. Zhang, Y. Yang, B. Li, J. Li, E. Ma, J.-F. Nie, Large plasticity in magnesium mediated by pyramidal dislocations, Science 365 (2019) 73–75.
[5] P.G. Partridge, The crystallography and deformation modes of hexagonal close-packed metals, Metall. Rev. 12 (1967) 169–194.
[6] M.H. Yoo, Slip, twinning, and fracture in hexagonal close-packed metals, Metall. Trans. a-Phys. Metall. Mater. Sci. 12 (1981) 409–418.
[7] S.R. Agnew, M.H. Yoo, C.N. Tome, Application of texture simulation to understanding mechanical behavior of Mg and solid solution alloys containing Li or Y, Acta Mater. 49 (2001) 4277–4289.
[8] I.J. Beyerlein, L. Capolungo, P.E. Marshall, R.J. McCabe, C.N. Tome, Statistical analyses of deformation twinning in magnesium (vol 90, pg 2161, 2010), Philos. Mag. 90 (2010) 4073–4074.
[9] M.R. Barnett, Twinning and the ductility of magnesium alloys Part I: "Tension" twins, Mater. Sci. Eng. a-Struct. Mater. Prop. Microstruct. Process. 464 (2007) 1–7.
[10] E. Roberts, P. Partridge, The accommodation around {1012} < 1011 > twins in magnesium, Acta Metall. 14 (1966) 513–527.
[11] U.M. Chaudry, K. Hamad, J.-G. Kim, On the ductility of magnesium based materials: A mini review, J. Alloy. Compd. 792 (2019) 652–664.
[12] Z. Yang, J. Li, J. Zhang, G. Lorimer, J. Robson, Review on research and development of magnesium alloys, Acta Metall. Sin. (Engl. Lett.) 21 (2008) 313–328.
[13] B.C. Suh, M.S. Shim, K.S. Shin, N.J. Kim, Current issues in magnesium sheet alloys: Where do we go from here? Scr. Mater., 84- 85 (2014) 1–6.
[14] D. Griffiths, Explaining texture weakening and improved formability in magnesium rare earth alloys, Mater. Sci. Technol. 31 (2015) 10–24.
[15] M. Sanjari, A. Farzadfar, A. Kabir, H. Utsunomiya, I.-H. Jung, R. Petrov, L. Kestens, S. Yue, Promotion of texture weakening in magnesium by alloying and thermomechanical processing:(I) alloying, J. Mater. Sci. 49 (2014) 1408–1425.
[16] H. Ding, X. Shi, Y. Wang, G. Cheng, S. Kamado, Texture weakening and ductility variation of Mg–2Zn alloy with CA or RE addition, Mater. Sci. Eng.: A 645 (2015) 196–204.
[17] J. Xu, B. Guan, Y. Xin, G. Huang, P. Wu, Q. Liu, Revealing the role of pyramidal < c+ a > slip in the high ductility of Mg-Li alloy, J. Magnes. Alloy. (2021).
[18] Z. Ding, W. Liu, H. Sun, S. Li, D. Zhang, Y. Zhao, E.J. Lavernia, Y. Zhu, Origins and dissociation of pyramidal < c+ a > dislocations in magnesium and its alloys, Acta Mater. 146 (2018) 265–272.
[19] D.A. Basha, H. Somekawa, A. Singh, Crack propagation along grain boundaries and twins in Mg and Mg-0.3 at%Y alloy during in-situ straining in transmission electron microscope, Scr. Mater. 142 (2018) 50–54.
[20] H. Somekawa, A. Kinoshita, A. Kato, Effect of alloying elements on room temperature stretch formability in Mg alloys, Mater. Sci. Eng.: A 732 (2018) 21–28.
[21] S. Agnew, J. Horton, M. Yoo, Transmission electron microscopy investigation of 〈 c+ a〉 dislocations in Mg and α-solid solution Mg-Li alloys, Metall. Mater. Trans. A 33 (2002) 851–858.
[22] J. Bhattacharyya, F. Wang, P. McQuade, S. Agnew, Deformation and fracture behavior of Mg alloy, WE43, after various aging heat treatments, Mater. Sci. Eng.: A 705 (2017) 79–88.
[23] N. Stanford, R.K.W. Marceau, M.R. Barnett, The effect of high yttrium solute concentration on the twinning behaviour of magnesium alloys, Acta Mater. 82 (2015) 447–456.
[24] L. Gao, R. Chen, E. Han, Effects of rare-earth elements Gd and Y on the solid solution strengthening of Mg alloys, J. Alloy. Compd. 481 (2009) 379–384.
[25] J.A. Yasi, L.G. Hector Jr, D.R. Trinkle, First-principles data for solid-solution strengthening of magnesium: From geometry and chemistry to properties, Acta Mater. 58 (2010) 5704–5713.
[26] H. Zhou, G.M. Cheng, X.L. Ma, W.Z. Xu, S.N. Mathaudhu, Q.D. Wang, Y.T. Zhu, Effect of Ag on interfacial segregation in Mg-Gd-Y-(Ag)-Zr alloy, Acta Mater. 95 (2015) 20–29.

[27] B. Leu, M.A. Kumar, K. Xie, I.J. Beyerlein, Investigation of twin growth mechanisms in precipitate hardened AZ91, Acta Mater. (2022) 118471.
[28] B. Leu, M.A. Kumar, K.Y. Xie, I.J. Beyerlein, Twinning pathways enabled by precipitates in AZ91, Materialia 21 (2022) 101292.
[29] J. Wang, X. Wang, K. Yu, T.J. Rupert, S. Mahajan, E.J. Lavernia, J.M. Schoenung, I.J. Beyerlein, Manipulating deformation mechanisms with Y alloying of Mg, Mater. Sci. Eng.: A 817 (2021) 141373.
[30] J. Han, X. Su, Z.-H. Jin, Y. Zhu, Basal-plane stacking-fault energies of Mg: A first-principles study of Li-and Al-alloying effects, Scr. Mater. 64 (2011) 693–696.
[31] Z. Wu, W. Curtin, Mechanism and energetics of⟨ c+ a⟩ dislocation cross-slip in hcp metals, Proceedings of the National Academy of Sciences, 113 (2016) 11137–11142.
[32] M.H. Yoo, J.K. Lee, Deformation Twinning in Hcp Metals and Alloys, Philos. Mag. a-Phys. Condens. Matter Struct. Defects Mech. Prop. 63 (1991) 987–1000.
[33] J. Wang, I.J. Beyerlein, C.N. Tome, An atomic and probabilistic perspective on twin nucleation in Mg, Scr. Mater. 63 (2010) 741–746.
[34] M.A. Kumar, L. Capolungo, R.J. McCabe, C.N. Tomé, Characterizing the role of adjoining twins at grain boundaries in hexagonal close packed materials, Sci. Rep. 9 (2019) 3846.
[35] M. Gharghouri, G. Weatherly, J. Embury, The interaction of twins and precipitates in a Mg-7.7 at% Al alloy, Philos. Mag. A 78 (1998) 1137–1149.
[36] J. Robson, The effect of internal stresses due to precipitates on twin growth in magnesium, Acta Mater. 121 (2016) 277–287.
[37] K.Y. Xie, D. Zhao, B. Leu, X. Ma, Q. Jiao, J.A. El-Awady, T.P. Weihs, I.J. Beyerlein, M.A. Kumar, Understanding the interaction of extension twinning and basal-plate precipitates in Mg-9Al using precession electron diffraction, Materialia 15 (2021) 101044.
[38] C. Guo, R. Xin, G. Wu, F. Liu, G. Hu, Q. Liu, Observation of twin transmission process in Mg alloys by in situ EBSD, Adv. Eng. Mater. 21 (2019) 1801340.
[39] M.A. Kumar, I.J. Beyerlein, R.J. McCabe, C.N. Tome, Grain neighbour effects on twin transmission in hexagonal close-packed materials, Nat. Commun. 7 (2016) 13826(Article).
[40] M.A. Kumar, R. McCabe, C. Tomé, L. Capolungo, Geometric compatibility measure m′for twin transmission: a predictor or descriptor?, Materials Today, Communications (2022) 104634.
[41] M.A. Kumar, K. Dang, V. Taupin, R. McCabe, C. Tomé, L. Capolungo, Numerical and experimental characterization of twin transmission across grain boundaries along the forward and lateral directions, Materialia 23 (2022) 101437.
[42] F. Mokdad, D.L. Chen, D.Y. Li, Twin-twin interactions and contraction twin formation in an extruded magnesium alloy subjected to an alteration of compressive direction, J. Alloy. Compd. 737 (2018) 549–560.
[43] Q. Yu, J. Wang, Y.Y. Jiang, R.J. McCabe, N. Li, C.N. Tome, Twin-twin interactions in magnesium, Acta Mater. 77 (2014) 28–42.
[44] D. Shi, T. Liu, T. Wang, D. Hou, S. Zhao, S. Hussain, {10–12} Twins across twin boundaries traced by in situ EBSD, J. Alloy. Compd. 690 (2017) 699–706.
[45] B. Kondori, A. Benzerga, Effect of stress triaxiality on the flow and fracture of Mg alloy AZ31, Metall. Mater. Trans. A 45 (2014) 3292–3307.
[46] D. Xu, E. Han, Relationship between fatigue crack initiation and activated {101¯2} twins in as-extruded pure magnesium, Scr. Mater. 69 (2013) 702–705.
[47] J.-Y. Kim, K.-T. Yoo, J.-W. Byeon, Tension twin-induced premature fracture mechanism of aging-treated AZ91D magnesium alloy, Mater. Charact. 172 (2021) 110865.
[48] L. Li, J. Yang, Z. Yang, Q. Sun, L. Tan, Q. Zeng, M. Zhu, Towards revealing the relationship between deformation twin and fatigue crack initiation in a rolled magnesium alloy, Mater. Charact. 179 (2021) 111362.
[49] N. Grilli, A.C. Cocks, E. Tarleton, Modelling the nucleation and propagation of cracks at twin boundaries, Int. J. Fract. 233 (2022) 17–38.
[50] N. Grilli, E. Tarleton, A.C. Cocks, Coupling a discrete twin model with cohesive elements to understand twin-induced fracture, Int. J. Fract. 227 (2021) 173–192.
[51] Q. Yu, Y. Jiang, J. Wang, Cyclic deformation and fatigue damage in single-crystal magnesium under fully reversed strain-controlled tension–compression in the [100] direction, Scr. Mater. 96 (2015) 41–44.
[52] H. El Kadiri, J. Kapil, A.L. Oppedal, L.G. Hector, S.R. Agnew, M. Cherkaoui, S.C. Vogel, The effect of twin-twin interactions on the nucleation and propagation of {10(1)over-bar2} twinning in magnesium, Acta Mater. 61 (2013) 3549–3563.
[53] H. Chen, T. Liu, S. Xiang, Y. Liang, Abnormal migration of twin boundaries in rolled AZ31 alloy containing intersecting {101 2} extension twins, J. Alloy. Compd. 690 (2017) 376–380.
[54] B.M. Morrow, E.K. Cerreta, R.J. McCabe, C.N. Tome, Toward understanding twin-twin interactions in hcp metals: Utilizing multiscale techniques to characterize deformation mechanisms in magnesium, Mater. Sci. Eng. a-Struct. Mater. Prop. Microstruct. Process. 613 (2014) 365–371.
[55] B.M. Morrow, R.J. Mccabe, E.K. Cerreta, C.N. Tome, In-Situ TEM Observation of Twinning and Detwinning During Cyclic Loading in Mg, Metall. Mater. Trans. a-Phys. Metall. Mater. Sci. 45a (2014) 36–40.
[56] C. Reid, A review of mechanical twinning in body-centred cubic metals and its relation to brittle fracture, J. Less Common Met. 9 (1965) 105–122.
[57] C. Reid, The association of twinning and fracture in bcc metals, Metall. Trans. A 12 (1981) 371–377.
[58] W.D. Russell, N.R. Bratton, Y. Paudel, R.D. Moser, Z.B. McClelland, C.D. Barrett, A.L. Oppedal, W.R. Whittington, H. Rhee, S. Mujahid, In Situ Characterization of the Effect of Twin-Microstructure Interactions on {1 0 1 2} Tension and {1 0 1 1} Contraction Twin Nucleation, Growth and Damage in Magnesium, Metals 10 (2020) 1403.
[59] K. Zhang, Z. Shao, J. Jiang, Effects of twin-twin interactions and deformation bands on the nucleation of recrystallization in AZ31 magnesium alloy, Mater. Des. 194 (2020) 108936.
[60] M. Lentz, M. Risse, N. Schaefer, W. Reimers, I.J. Beyerlein, Strength and ductility with {10-11} - {10-12} double twinning in a magnesium alloy, Nat. Commun. 7 (2016) 11068.
[61] Y.C. Xin, M.Y. Wang, Z. Zeng, M.G. Nie, Q. Liu, Strengthening and toughening of magnesium alloy by {10-12} extension twins, Scr. Mater. 66 (2012) 25–28.
[62] X. Wang, L. Jiang, C. Cooper, K. Yu, D. Zhang, T.J. Rupert, S. Mahajan, I.J. Beyerlein, E.J. Lavernia, J.M. Schoenung, Toughening magnesium with gradient twin meshes, Acta Mater. 195 (2020) 468–481.
[63] Q. Zhang, J. Li, K. Jiang, P. Li, Y. Li, Y. Zhang, T. Suo, Gradient structure induced simultaneous enhancement of strength and ductility in AZ31 Mg alloy with twin-twin interactions, J. Magnes. Alloy. (2021).
[64] M. Lentz, M. Klaus, I.J. Beyerlein, M. Zecevic, W. Reimers, M. Knezevic, In situ X-ray diffraction and crystal plasticity modeling of the deformation behavior of extruded Mg-Li-(Al) alloys: An uncommon tension-compression asymmetry, Acta Mater. 86 (2015) 254–268.
[65] Q. Yu, J. Wang, Y.Y. Jiang, R.J. McCabe, C.N. Tome, Co-zone {(1)over-bar012} Twin Interaction in Magnesium Single Crystal, Mater. Res. Lett. 2 (2014) 82–88.
[66] M. Gong, W. Wu, Atomic-level study of twin–twin interactions in hexagonal metals, J. Mater. Res. 35 (2020) 1647–1659.
[67] M. Gong, S. Xu, Y. Jiang, Y. Liu, J. Wang, Structural characteristics of {1¯012} non-cozone twin-twin interactions in magnesium, Acta Mater. 159 (2018) 65–76.
[68] M.A. Kumar, M. Gong, I. Beyerlein, J. Wang, C.N. Tomé, Role of local stresses on co-zone twin-twin junction formation in HCP magnesium, Acta Mater. 168 (2019) 353–361.
[69] C. Barrett, J. Martinez, M. Nitol, Faceting and Twin–Twin Interactions in {11 2 1} and {11 2 2} Twins in Titanium, Metals 12 (2022) 895.
[70] K. Dang, C.N. Tomé, L. Capolungo, The {101¯2} non-cozone twin-twin interactions in Mg: A stability and mobility study using 3-D atomistic simulations, Scr. Mater. 200 (2021) 113913.
[71] B. Leu, M.A. Kumar, I.J. Beyerlein, The effects of free surfaces on deformation twinning in HCP metals, Materialia 17 (2021) 101124.
[72] M.A. Kumar, I.J. Beyerlein, Local micromechanical fields and deformation twinning microstructure development in HCP crystals, J. Mater. Res. 35 (2020) 217–241.
[73] M.A. Kumar, I.J. Beyerlein, C.N. Tome, Effect of local stress fields on twin characteristics in HCP metals, Acta Mater. 116 (2016) 143–154.
[74] M.A. Kumar, A.K. Kanjarla, S.R. Niezgoda, R.A. Lebensohn, C.N. Tome, Numerical study of the stress state of a deformation twin in magnesium, Acta Mater. 84 (2015) 349–358.
[75] H. Moulinec, P. Suquet, A numerical method for computing the overall response of nonlinear composites with complex microstructure, Comput. Methods Appl. Mech. Eng. 157 (1998) 69–94.
[76] R.A. Lebensohn, N-site modeling of a 3D viscoplastic polycrystal using Fast Fourier Transform, Acta Mater. 49 (2001) 2723–2737.
[77] R. Brenner, R. Lebensohn, O. Castelnau, Elastic anisotropy and yield surface estimates of polycrystals, Int. J. Solids Struct. 46 (2009) 3018–3026.
[78] R.A. Lebensohn, R. Brenner, O. Castelnau, A.D. Rollett, Orientation image-based micromechanical modelling of subgrain texture evolution in polycrystalline copper, Acta Mater. 56 (2008) 3914–3926.
[79] R.A. Lebensohn, A.K. Kanjarla, P. Eisenlohr, An elasto-viscoplastic formulation based on fast Fourier transforms for the prediction of micromechanical fields in polycrystalline materials, Int. J. Plast., 32- 33 (2012) 59–69.
[80] I.J. Beyerlein, C.N. Tome, A dislocation-based constitutive law for pure Zr including temperature effects, Int. J. Plast. 24 (2008) 867–895.
[81] B. Leu, M.A. Kumar, P.F. Rottmann, K.J. Hemker, I.J. Beyerlein, Micromechanical Fields Associated with Irregular Deformation Twins in Magnesium, J. Mater. Eng. Perform. (2022) 1–12.
[82] M. Rakshith, P. Seenuvasaperumal, Review on the effect of different processing techniques on the microstructure and mechanical behaviour of AZ31 Magnesium alloy, J. Magnes. Alloy. 9 (2021) 1692–1714.
[83] D.W. Shu, I.R. Ahmad, Magnesium alloys: an alternative for aluminium in structural applications, in: Advanced Materials Research, Trans Tech Publ, 2011, pp. 1631–1635.
[84] A. Musfirah, A. Jaharah, Magnesium and aluminum alloys in automotive industry, J. Appl. Sci. Res. 8 (2012) 4865–4875.
[85] A.M. Becerra Correa, Effect of solute elements on the lattice parameters of magnesium, in, McGill University, 2006.
[86] G. Simmons, H. Wang, Single Crystal Elastic Constants and Calculated Aggregate Properties: A Handbook, MIT press,, 1971.
[87] I.J. Beyerlein, R.J. McCabe, C.N. Tome, Effect of microstructure on the nucleation of deformation twins in polycrystalline high-purity magnesium: A multi-scale modeling study, J. Mech. Phys. Solids 59 (2011) 988–1003.
[88] M. Ardeljan, I.J. Beyerlein, B.A. McWilliams, M. Knezevic, Strain rate and temperature sensitive multi-level crystal plasticity model for large plastic deformation behavior: Application to AZ31 magnesium alloy, Int. J. Plast. 83 (2016) 90–109.
[89] Q. Yu, L. Qi, R.K. Mishra, J. Li, A.M. Minor, Reducing deformation anisotropy to achieve ultrahigh strength and ductility in Mg at the nanoscale, Proceedings of the National Academy of Sciences, 110, 2013: 13289–13293.
[90] M.A. Kumar, I.J. Beyerlein, R.A. Lebensohn, C.N. Tome, Modeling the effect of alloying elements in magnesium on deformation twin characteristics, Magnes. Technol. 2017 (2017) 159–165.

[91] M.A. Kumar, I.J. Beyerlein, R.A. Lebensohn, C.N. Tome, Role of alloying elements on twin growth and twin transmission in magnesium alloys, Mater. Sci. Eng. a-Struct. Mater. Prop. Microstruct. Process. 706 (2017) 295–303.
[92] M.A. Kumar, I.J. Beyerlein, C.N. Tome, A measure of plastic anisotropy for hexagonal close packed metals: Application to alloying effects on the formability of Mg, J. Alloy. Compd. 695 (2017) 1488–1497.
[93] M.Y. Gong, S. Xu, Y. Jiang, Y. Liu, J. Wang, Structural Characteristics of {1¯012} Non-cozone Twin-Twin Interactions in Magnesium, Acta Mater. (2018).
[94] P.A. Juan, C. Pradalier, S. Berbenni, R.J. McCabe, C.N. Tome, L. Capolungo, A statistical analysis of the influence of microstructure and twin-twin junctions on twin nucleation and twin growth in Zr, Acta Mater. 95 (2015) 399–410.
[95] Q. Sun, X. Zhang, Y. Ren, L. Tan, J. Tu, Observations on the intersection between 10T2 twin variants sharing the same zone axis in deformed magnesium alloy, Mater. Charact. 109 (2015) 160–163.
[96] E. Sukedai, T. Yokoyama, Investigation of tensile–compressive yield asymmetry and the role of deformation twin in extruded pure magnesium, Int. J. Mater. Res. 101 (2010) 736–740.
[97] E. Yukutake, J. Kaneko, M. Sugamata, Anisotropy and non-uniformity in plastic behavior of AZ31 magnesium alloy plates, Mater. Trans. 44 (2003) 452–457.
[98] M. Lentz, R.S. Coelho, B. Camin, C. Fahrenson, N. Schaefer, S. Selve, T. Link, I.J. Beyerlein, W. Reimers, In-situ, ex-situ EBSD and (HR-)TEM analyses of primary, secondary and tertiary twin development in an Mg-4 wt%Li alloy, Mater. Sci. Eng. a-Struct. Mater. Prop. Microstruct. Process. 610 (2014) 54–64.